Supplementary Information

Selective hydrogenation via precise hydrogen bond interactions on catalytic scaffolds

Song Shi[1,2§], Piaoping Yang[1§], Chaochao Dun[3], Weiqing Zheng[1], Jeffrey J. Urban[3], Dionisios G. Vlachos[1*]

[1] Department of Chemical and Biomolecular Engineering and Catalysis Center for Energy Innovation (CCEI), University of Delaware, Newark, DE 19716, USA.

[2] State Key Laboratory of Catalysis, Dalian Institute of Chemical Physics, Chinese Academy of Sciences, Dalian 116023, People's Republic of China.

[3] The Molecular Foundry, Lawrence Berkeley National Laboratory Berkeley, CA 94720(USA)

[§] These authors contributed equally.

email: vlachos@udel.edu

Table of contents

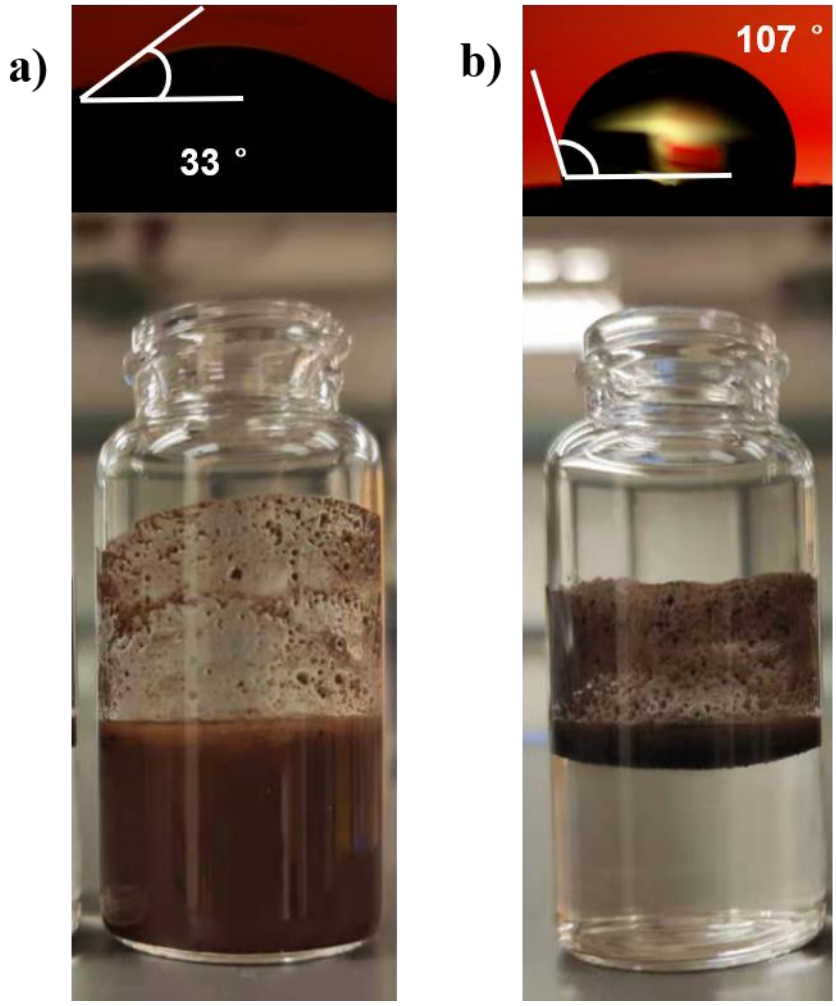

Figure S1. Wettability difference of support with different functional groups. HCP distribution difference on water and water contact angles. a) HCP-OH, b) HCP-CH_3.

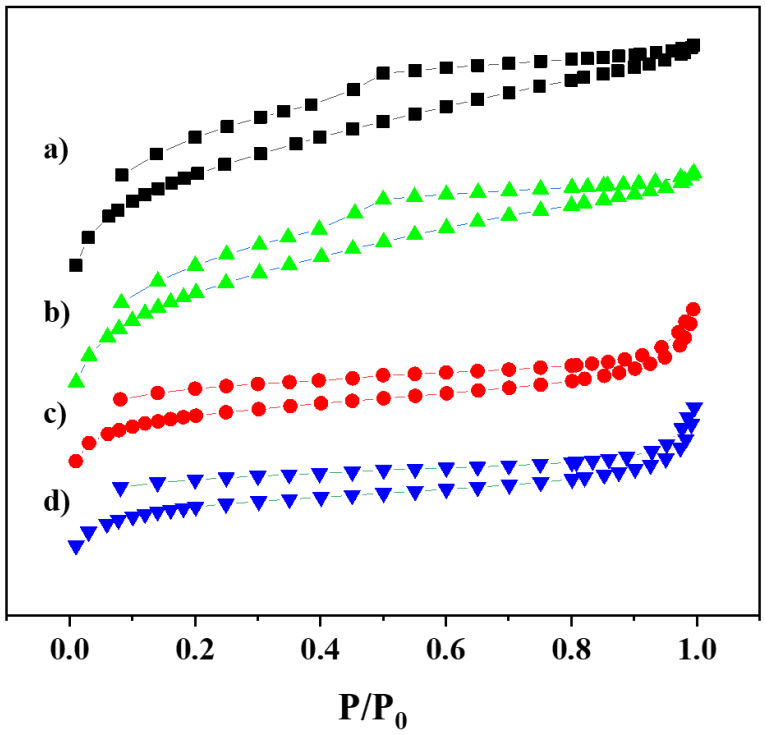

Figure S2. Pore structure comparison of different catalytic materials.

N_2 adsorption-desorption isotherms at 77 K. a) Ir-HCP-OH, b) HCP-OH, c) Ir-HCP-CH_3, d) HCP-CH_3.

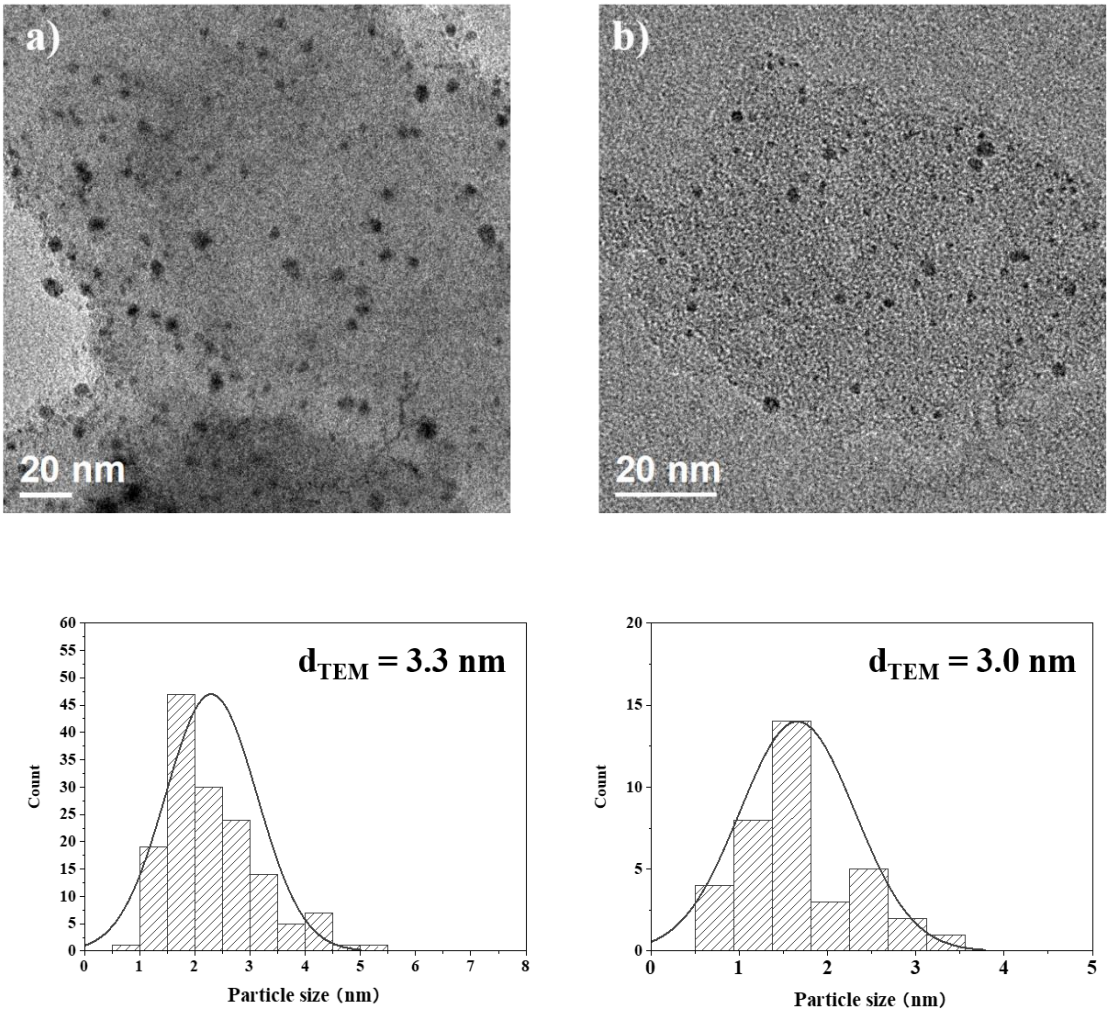

$$d_{TEM} = \sum n_i d_i^3 / \sum n_i d_i^2 \qquad \textbf{equation S1}$$

Figure S3. Ir particle size. TEM images and particle size distribution of a) Ir-HCP-OH and b) Ir-HCP-CH_3.

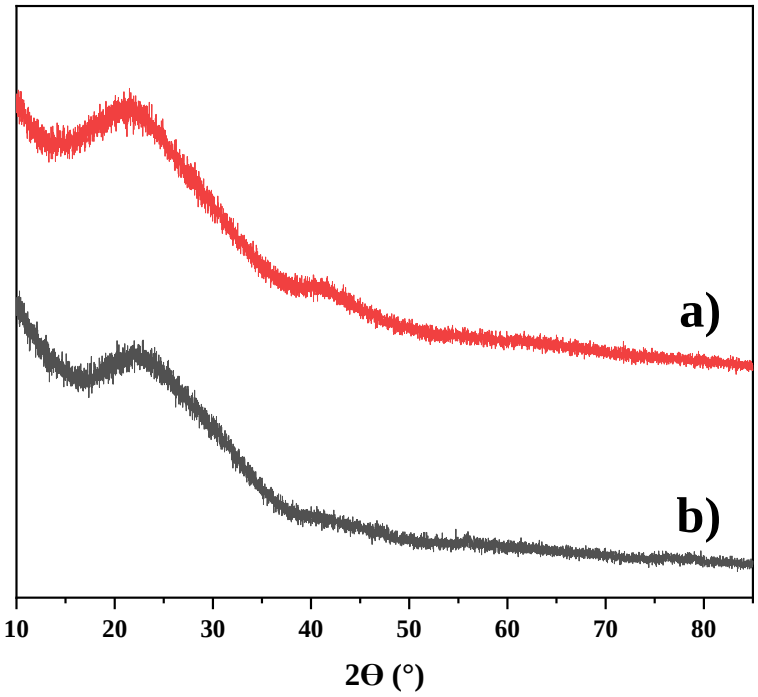

Figure S4. Crystallinity of supports. XRD patterns of a) HCP-CH_3 and b) HCP-OH.

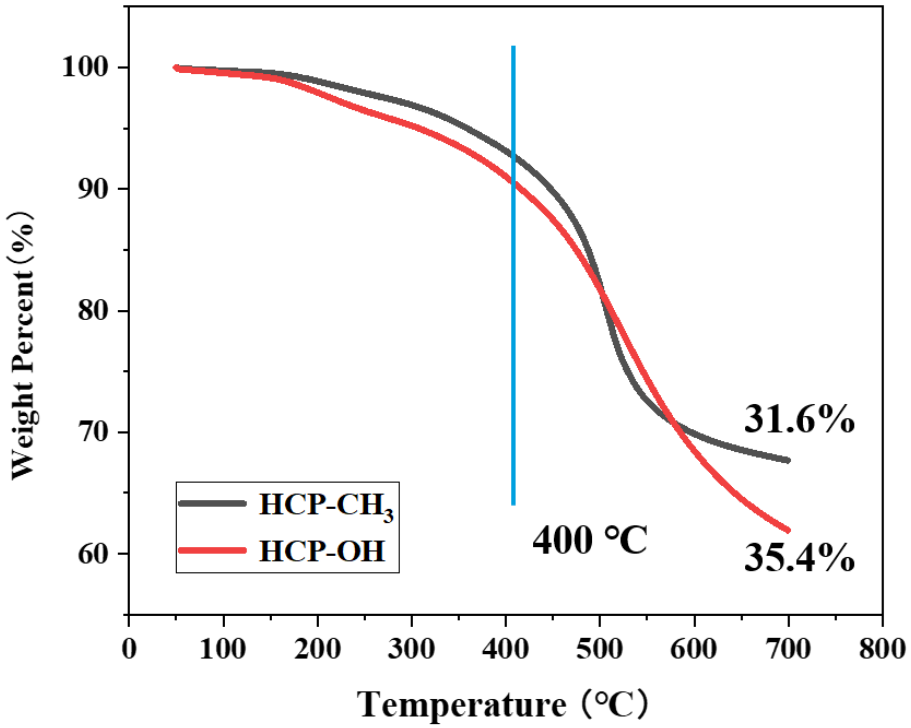

Figure S5. Thermal stability of the two catalysts. TGA curves of HCP-OH and HCP-CH_3.

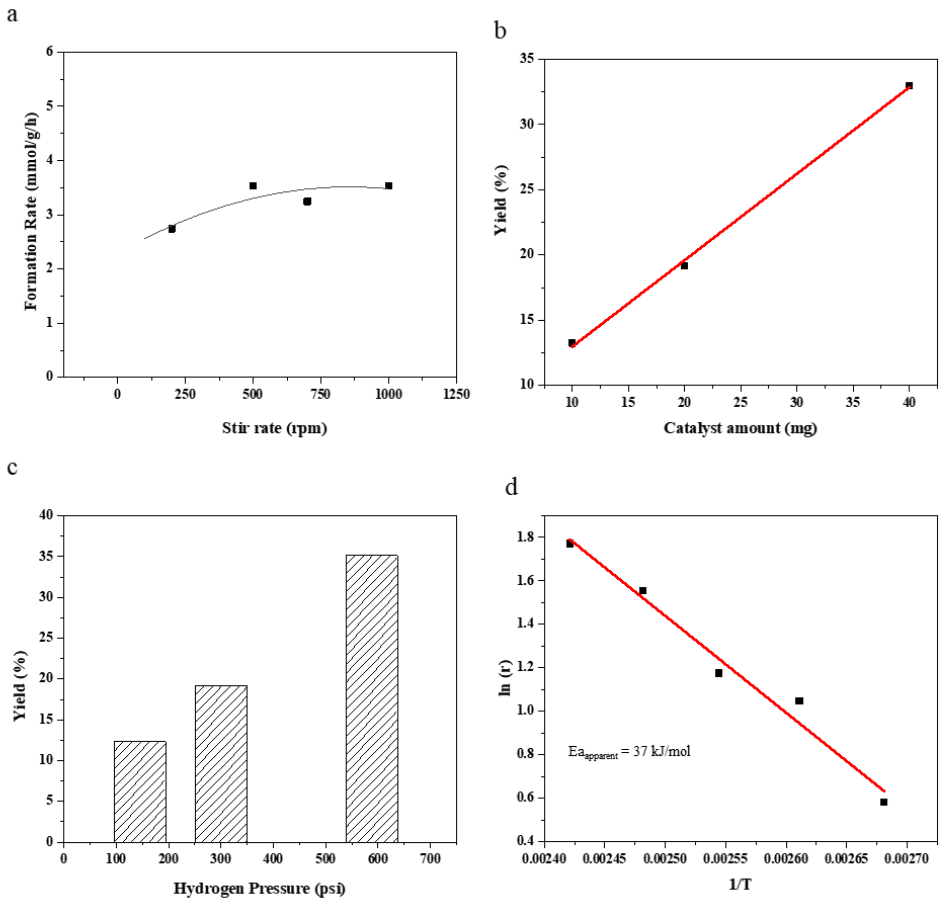

Figure S6. Kinetics and conditions for optimizing the reaction. a), Stir rate effect on rate with Ir-HCP-OH, b), catalyst amount effect with Ir-HCP-OH, c), hydrogen pressure effect with Ir-HCP-OH, d), Arrhenius plot of Ir-HCP-OH in furfural hydrogenation.

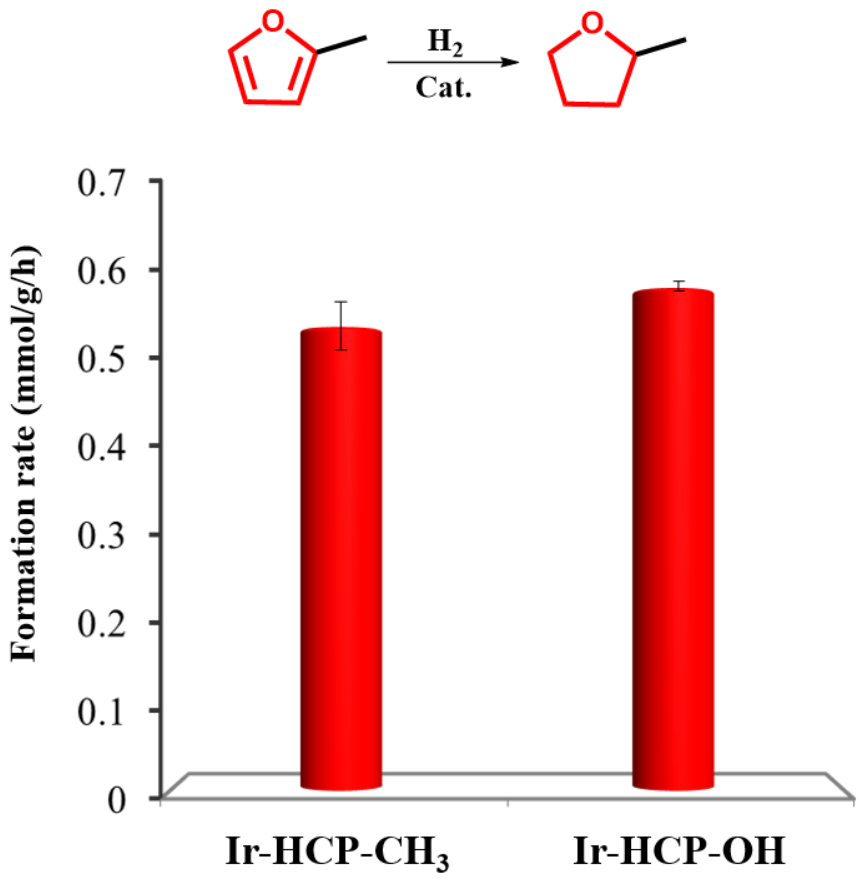

Figure S7. Reaction of 2-methylfuran. Hydrogenation rate over Ir-HCP-CH_3 and Ir-HCP-OH. Reaction conditions: substrate, 1 mmol; catalyst, 40 mg; hexane, 10 mL; H_2, 300 psi; 120 ℃.

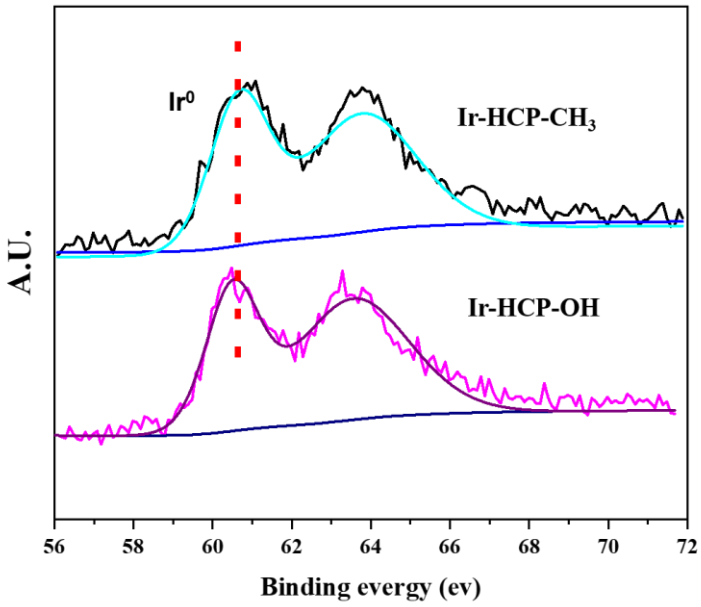

Figure S8. Electronic state of Ir over different supports via XPS. Ir *4f* of Ir-HCP-CH_3 and Ir-HCP-OH.

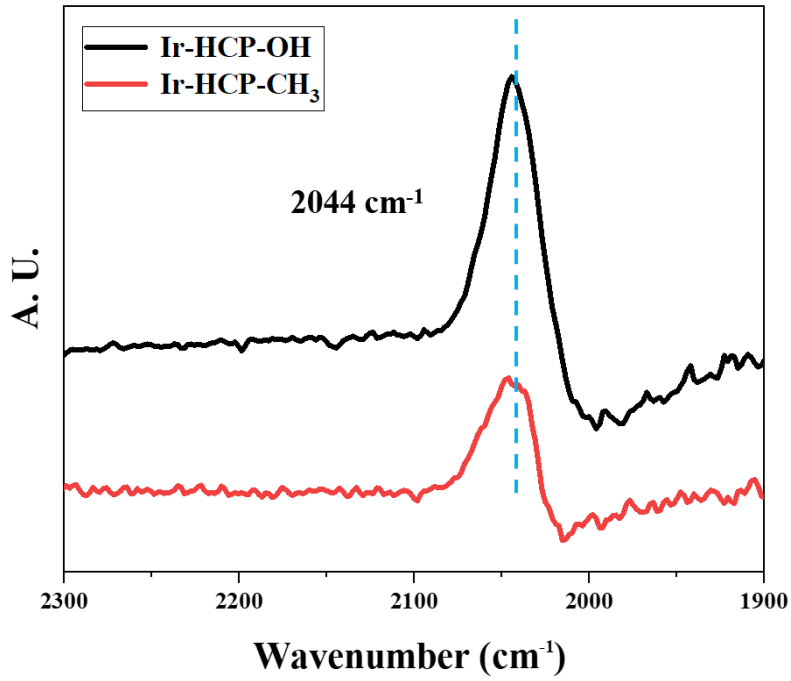

Figure S9. Electronic state of Ir over different supports via CO adsorption. *In situ* CO adsorption Drifts-IR peaks over Ir-HCP-CH_3 and Ir-HCP-OH.

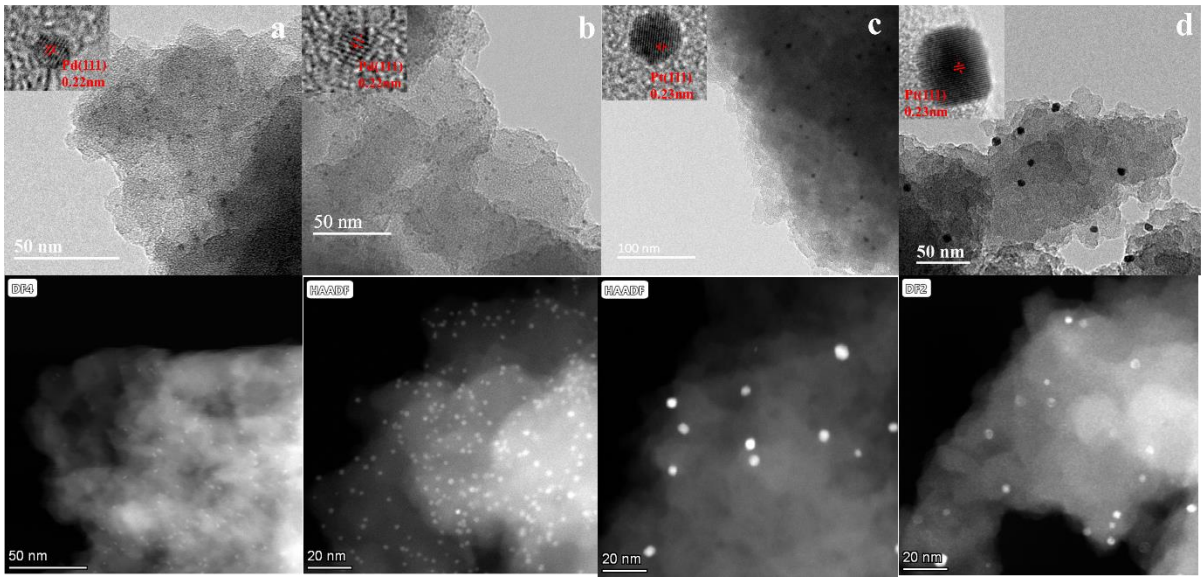

Figure S10. Microscopy characterization of Pd and Pt catalyst. TEM, HR-TEM and HAADF of a, Pd-HCP-CH_3, b, Pd-HCP-OH, c, Pt-HCP-CH_3, d, Pt-HCP-OH.

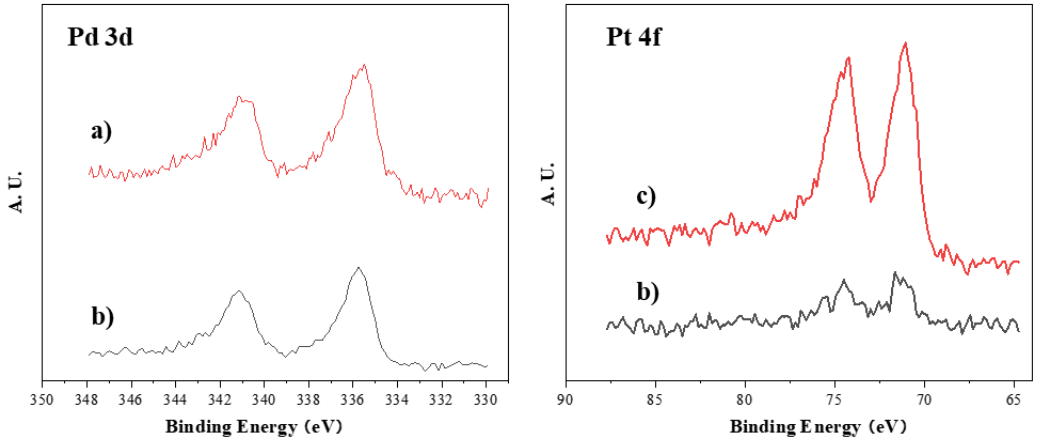

Figure S11. XPS spectra of the Pd and Pt catalysts, a) Pd-HCP-CH_3, b) Pd-HCP-OH, c) Pt-HCP-CH_3, and d) Pt-HCP-OH.

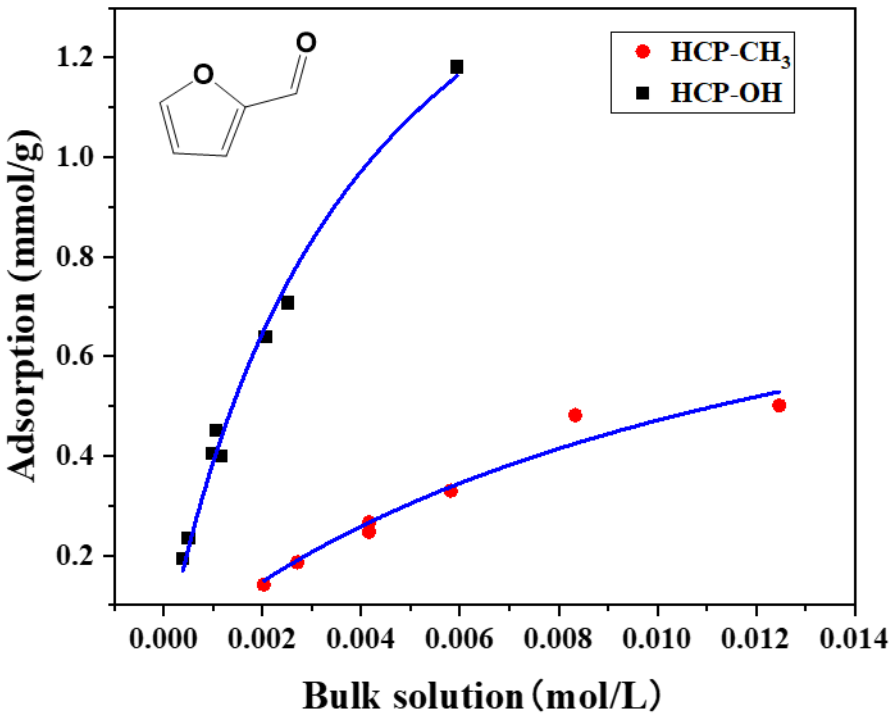

Furfural	Qmax (mmol/g)	K
HCP-OH	1.95 ±0.15	247±32
HCP-CH_3	1.05 ± 0.19	82±24

Figure S12. Adsorption isotherm of furfural on different supports. Results on HCP-OH and HCP-CH_3. Q_{max} and K are the saturated adsorption amount and affinity constant based on a Langmuir fit.

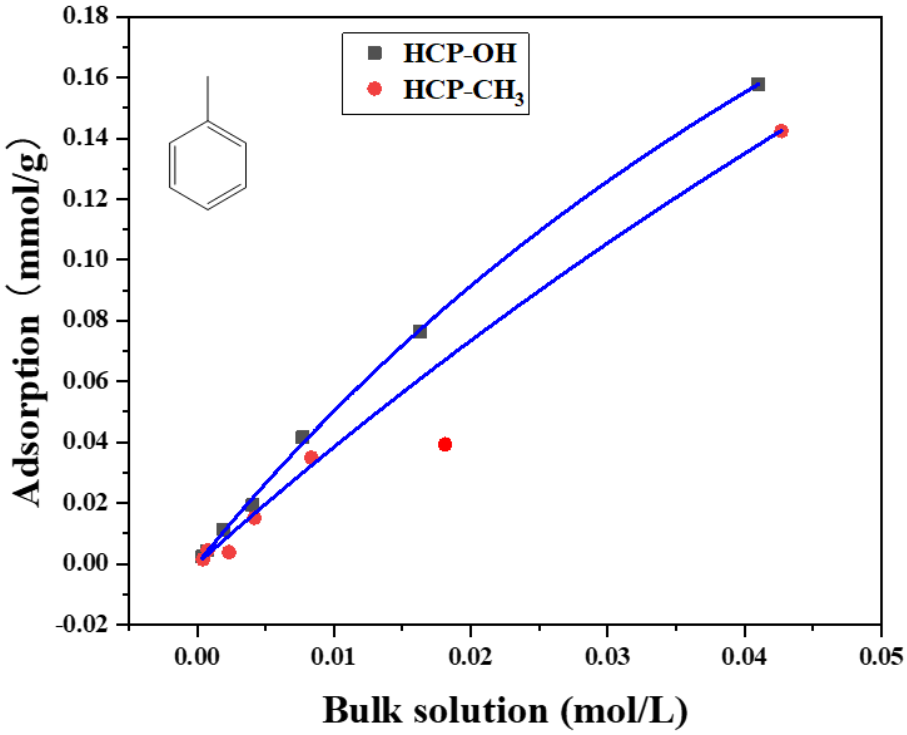

Toluene	Qmax (mmol/g)	K
HCP-OH	0.51±0.04	10.9±1
HCP-CH_3	0.83±0.44	4.9±3

Figure S13. Adsorption of toluene on HCP-OH and HCP-CH_3. Q_{max} and K are the saturated adsorption amount and affinity constant based on a Langmuir fit.

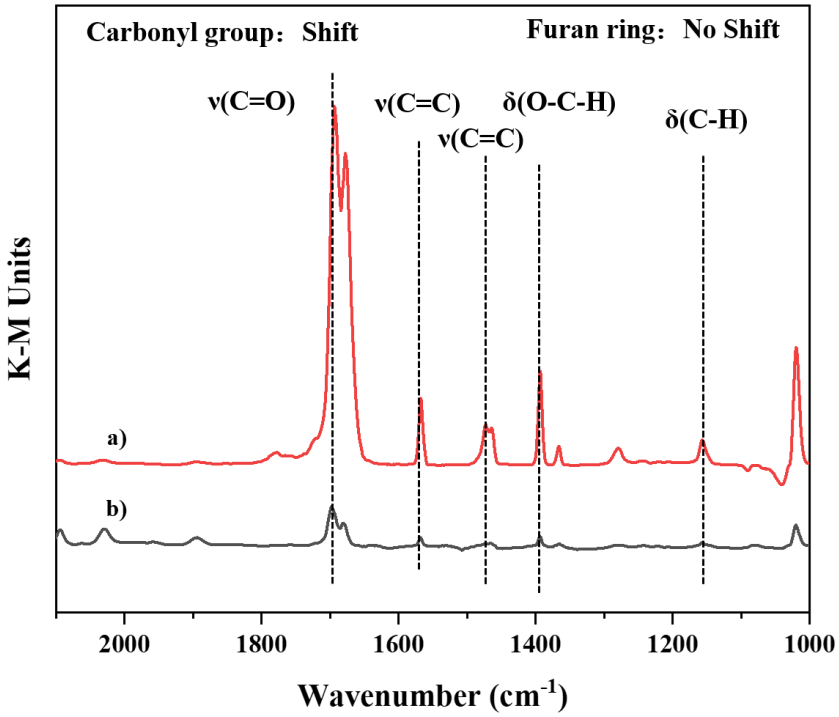

Figure S14. Interaction of furfural with different supports, using *in situ* Drifts IR adsorption. a) HCP-OH and b) HCP-CH_3 after the Kubelka-Munk (K-M) transformation.

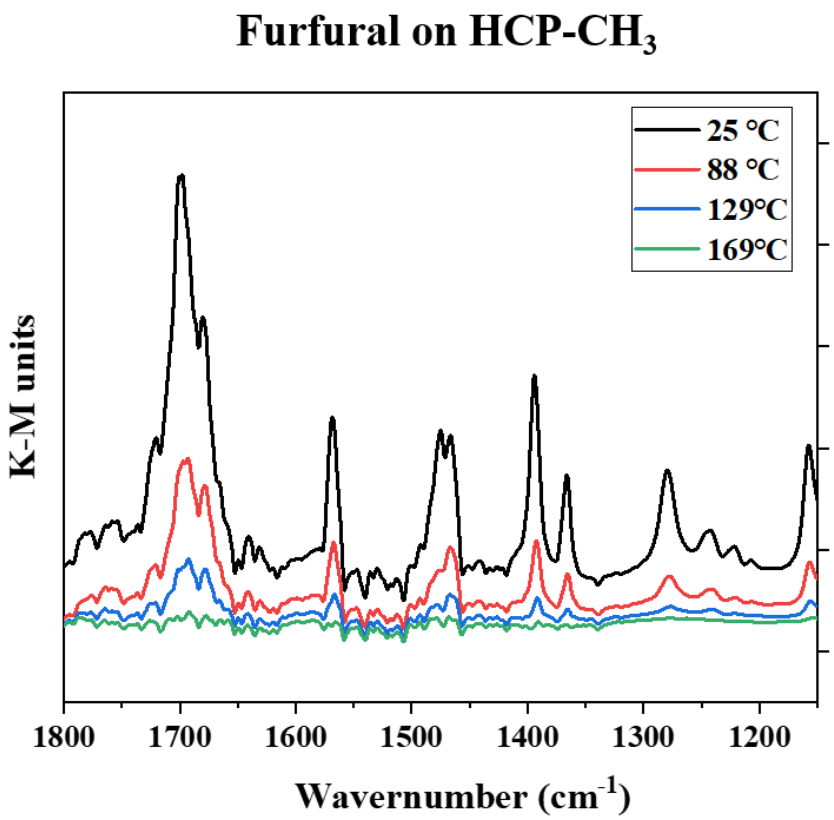

Figure S15. Interaction of furfural with HCP-CH_3 via *in situ* Drifts-IR TPD experiments. Results on HCP-CH_3 under different temperatures after the K-M transformation.

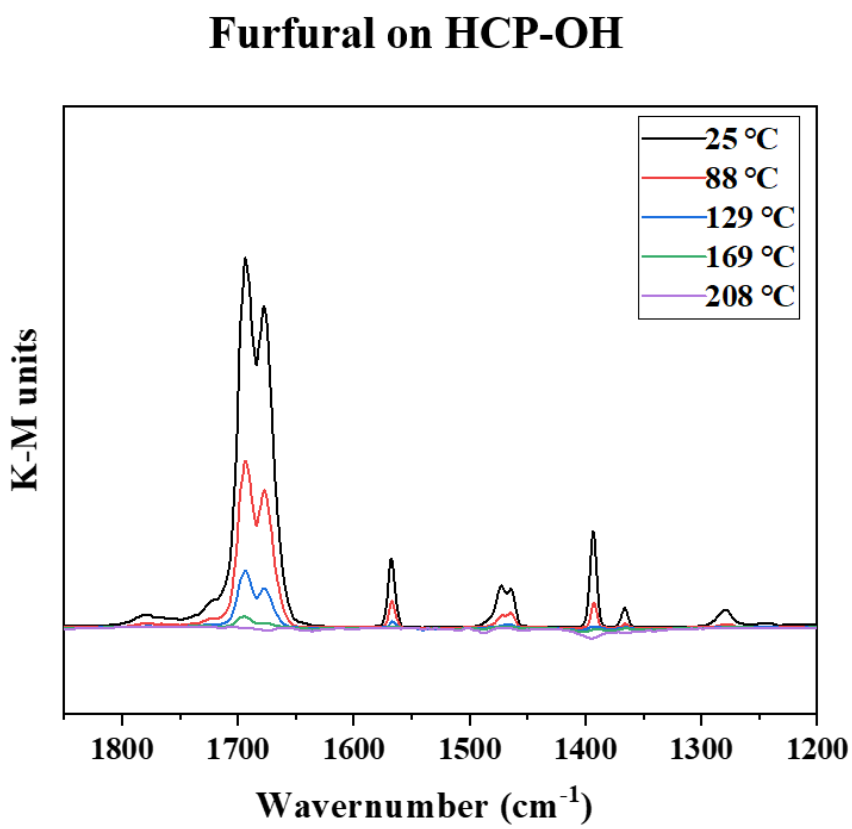

Figure S16. Interaction of furfural with HCP-OH, using *in situ* Drifts-IR TPD experiments. Drifts-IR of furfural on HCP-OH under different temperatures after the K-M transformation.

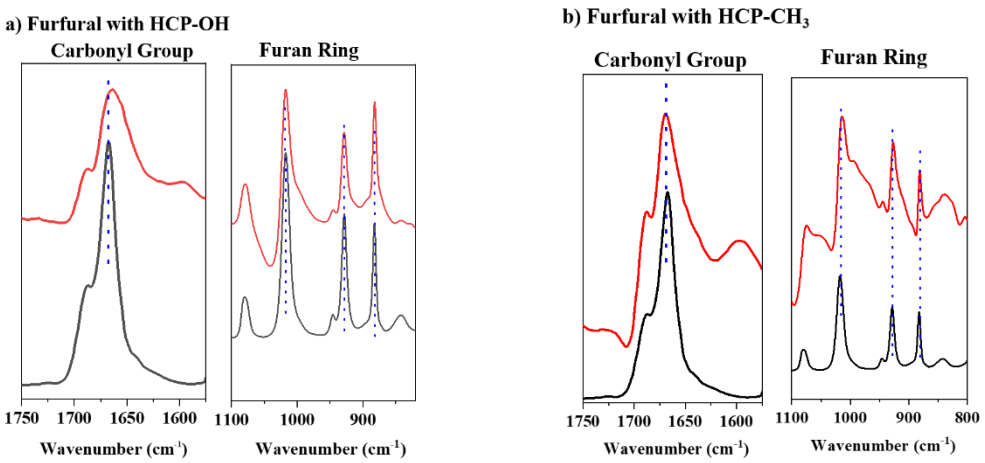

Figure S17. Interaction of furfural with different supports, using ATR-IR adsorption. a) HCP-OH and b) HCP-CH_3. Black line refers to the pure liquid furfural and the red line to furfural adsorbed on catalyst. Peaks at 1670 cm^{-1} are assigned to the carbonyl groups while those at 1018 cm^{-1}, 931 cm^{-1} and 886 cm^{-1} to the furan ring.

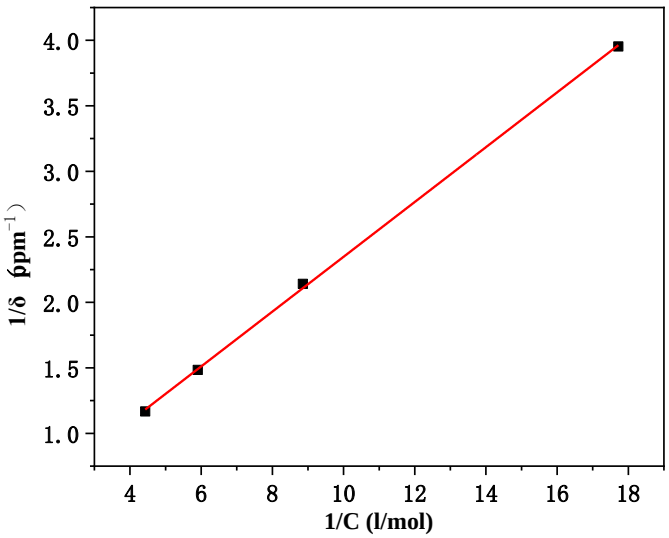

ratio	△δ（ppm）	δ（ppm）
0:1		4.5579
1:1	0.253	4.8109
2:1	0.4671	5.025
3:1	0.6739	5.2318
4:1	0.8566	5.4145
△G	-0.552 Kcal/mol	

$$1/\Delta\delta = a \times 1/K \times 1/C + a \qquad \text{equation S2}$$

$$\triangle G = -RT\ln(K) \qquad \text{equation S3}$$

Figure S18. Hydrogen bond measurement between furfural and phenol. Linear relationship between 1/Δδ and 1/C of furfural and phenol in $CDCl_3$, and chemical shift of active H in phenol with the addition of furfural.

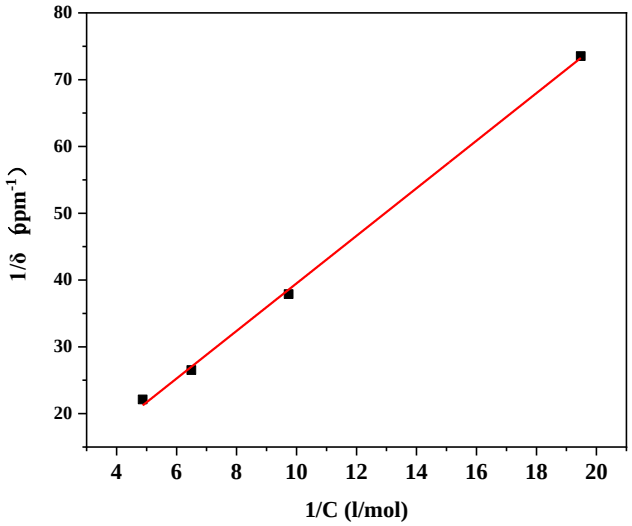

Ratio	△δ（ppm）	δ（ppm）
0:1		4.5579
1:1	0.0136	4.5715
2:1	0.0264	4.5843
3:1	0.0377	4.5956
4:1	0.0452	4.6031
△G	-0.213 Kcal/mol	

$$1/\Delta\delta = a \times 1/K \times 1/C + a \qquad \text{equation S2}$$

$$\triangle G = -RT\ln(K) \qquad \text{equation S3}$$

Figure S19. Hydrogen bond measurement between 2-MF and phenol.

Linear relationship between 1/Δδ and 1/C of 2-MF and phenol in $CDCl_3$, and chemical shift of active H in phenol with the addition of 2-MF.

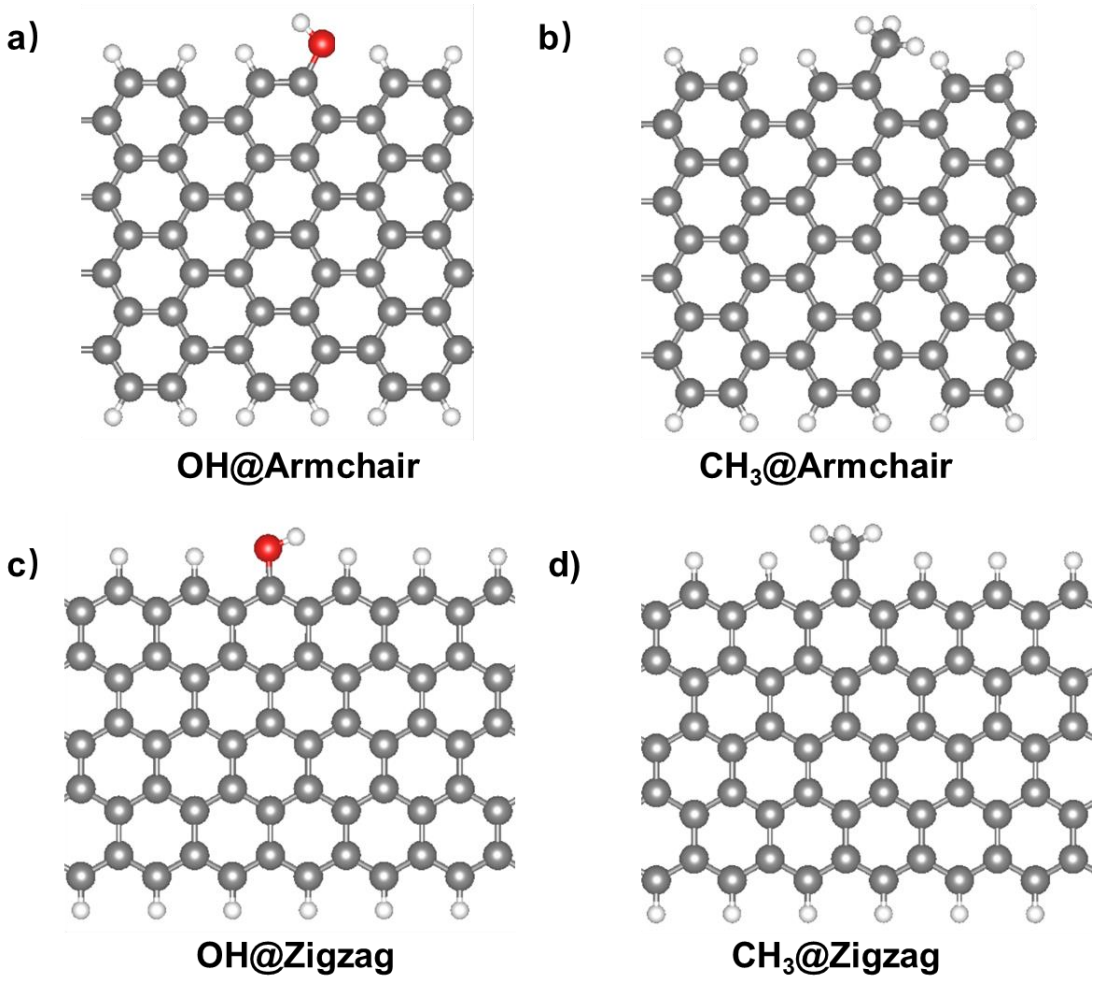

Figure S20. Computational models. (a) OH and (b) CH_3 on graphene ribbons with armchair edges; (c) OH and (d) CH_3 on graphene ribbons with zigzag edges.

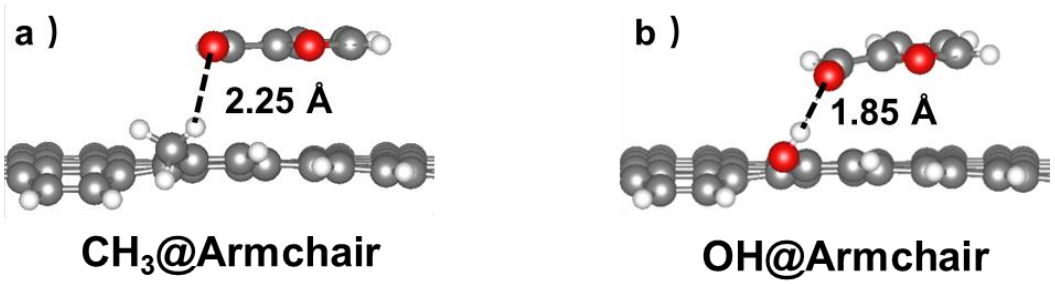

Figure S21. Optimized configurations of furfural adsorption over (a) CH_3 group and (b) OH group on armchair models.

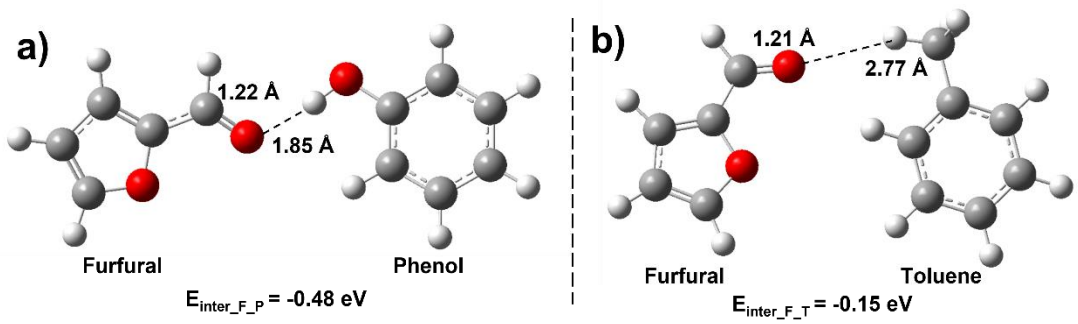

Figure S22. Optimized configurations of the interaction between furfural and monomers. (a) Furfural and Phenol; (b) Furfural and Toluene.

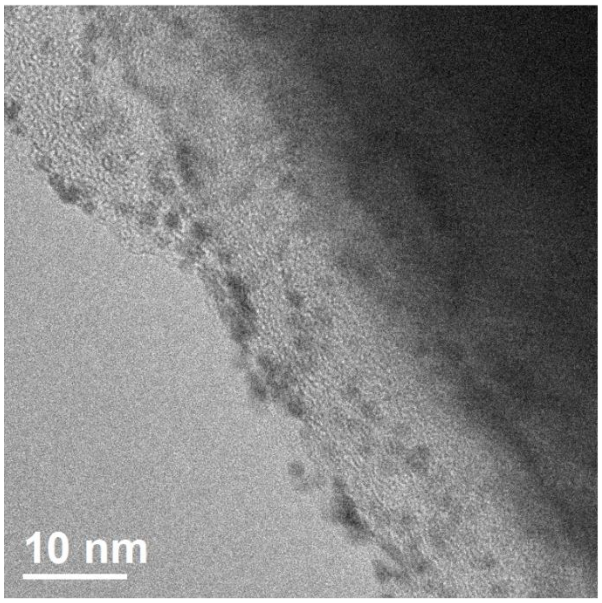

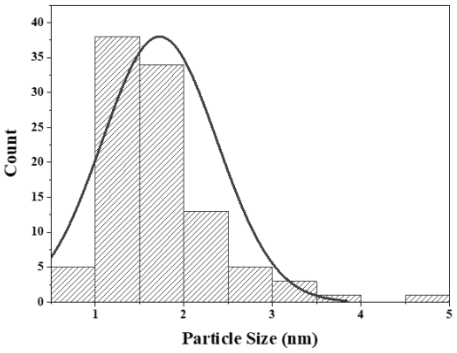

d_{TEM}=2.3 nm
Loading：0.2wt%

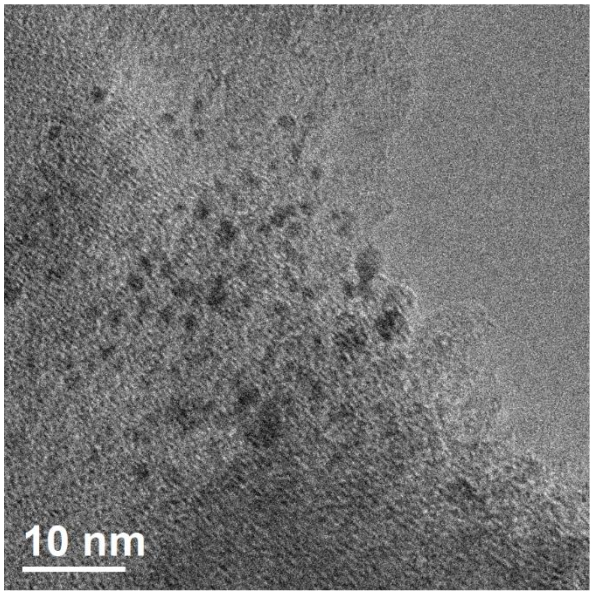

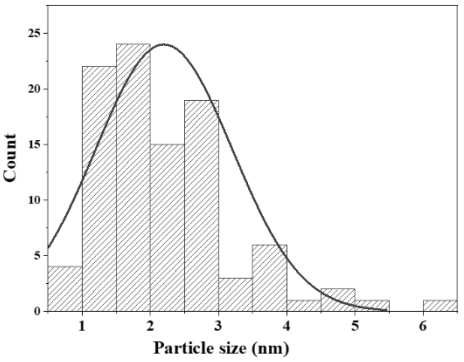

d_{TEM}=3.0 nm
Loading：0.5 wt%

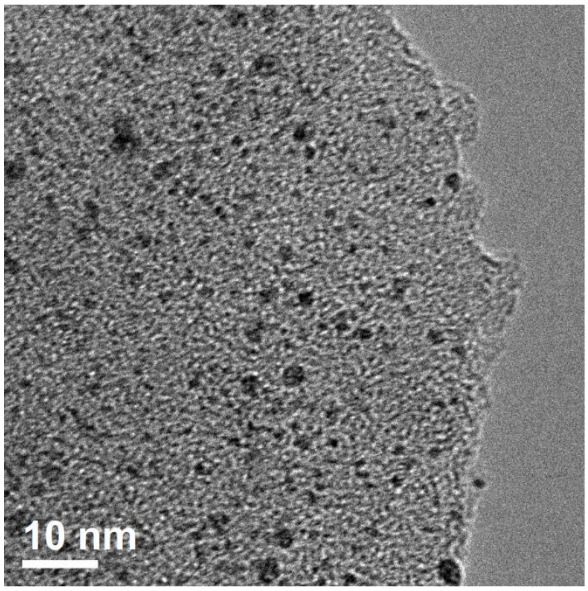

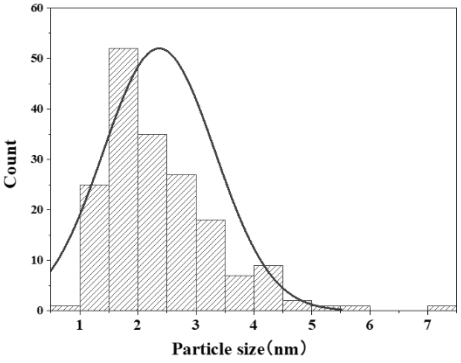

d_{TEM}=3.3 nm
Loading：1 wt%

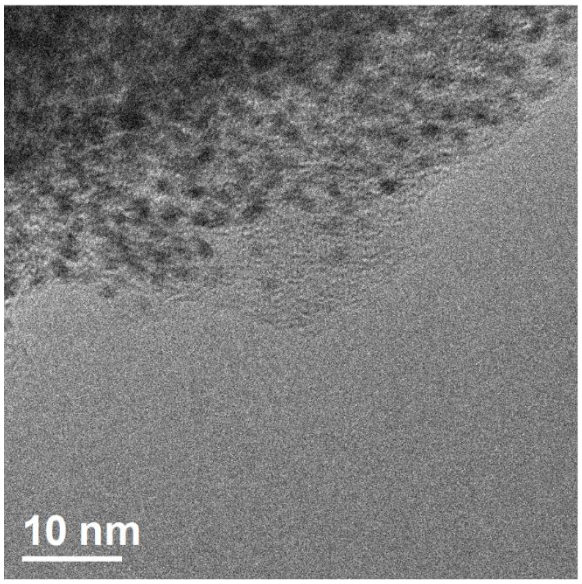

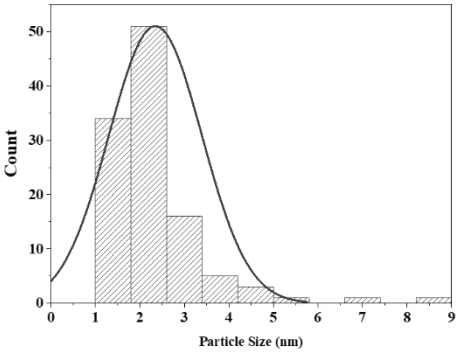

d_{TEM}=3.6 nm
Loading：2 wt%

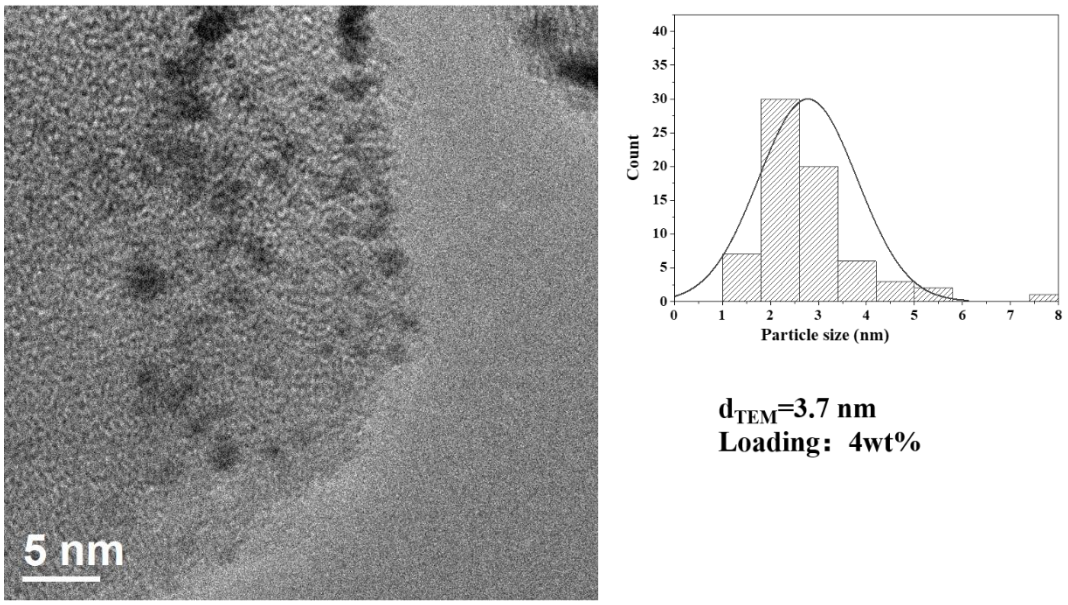

Figure S23. Particle size. TEM and particle size distribution of different Ir loading catalysts.

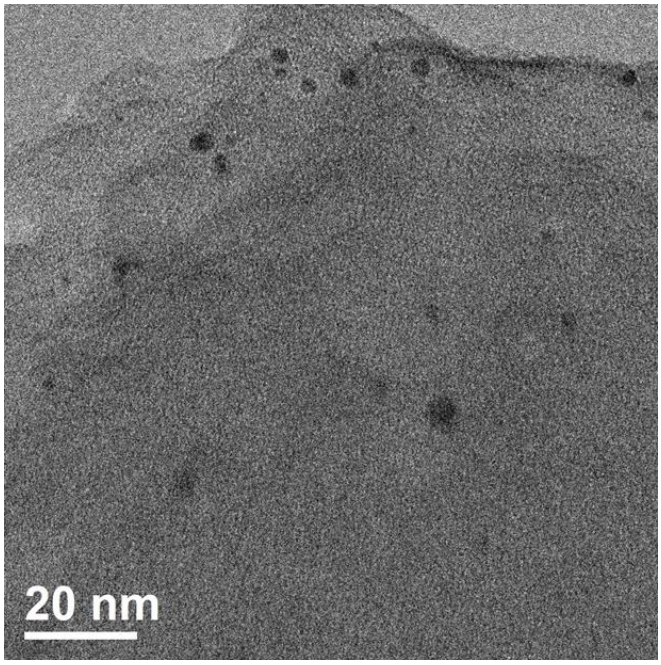

Figure S24. Ir particles after reaction. TEM images of Ir-HCP-OH after reaction.

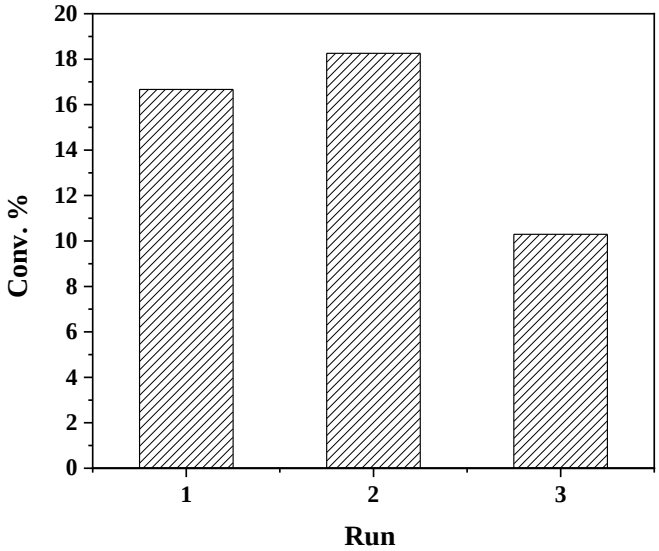

Figure S25. Catalyst reusability of Ir-HCP-OH.

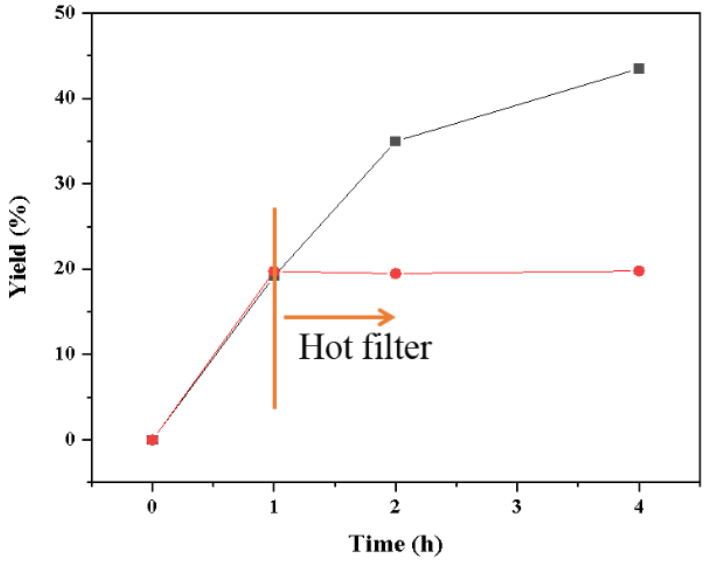

Figure S26. Hot filter experiment of furfural hydrogen with Ir-HCP-OH.

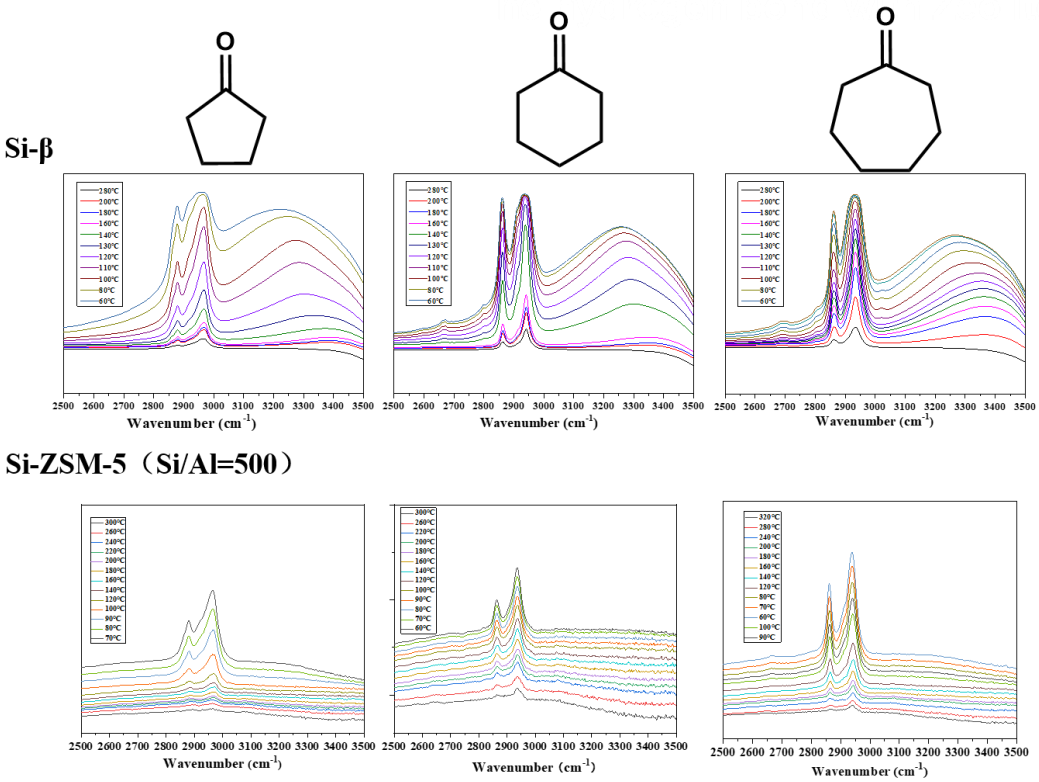

Figure S27. Ketone adsorption difference over different zeolites. *In situ* FT-IR of cyclopentanone, cyclohexanone, and cycloheptanone adsorption on Si-Beta and Si-ZSM-5 and corresponding TPD results.

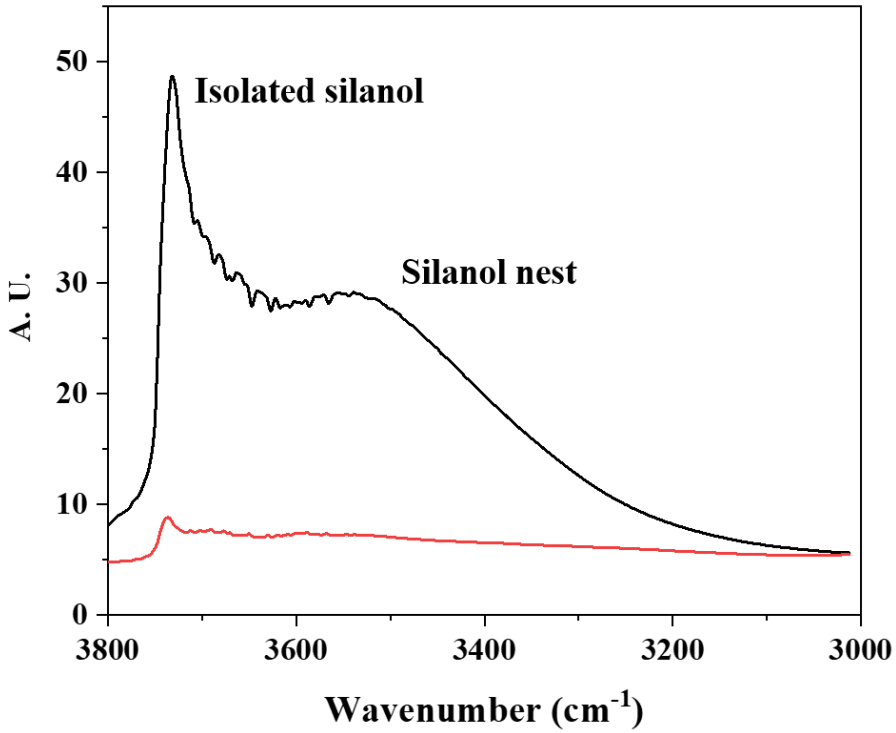

Figure S28. Surface hydroxy difference of Si-Beta and Si-ZSM-5. Drifts-IR after K-M transformation. Peaks at 3780 cm^{-1} assigned to isolated silanol and the broad peaks at 3500 cm^{-1} to the silanol nests.

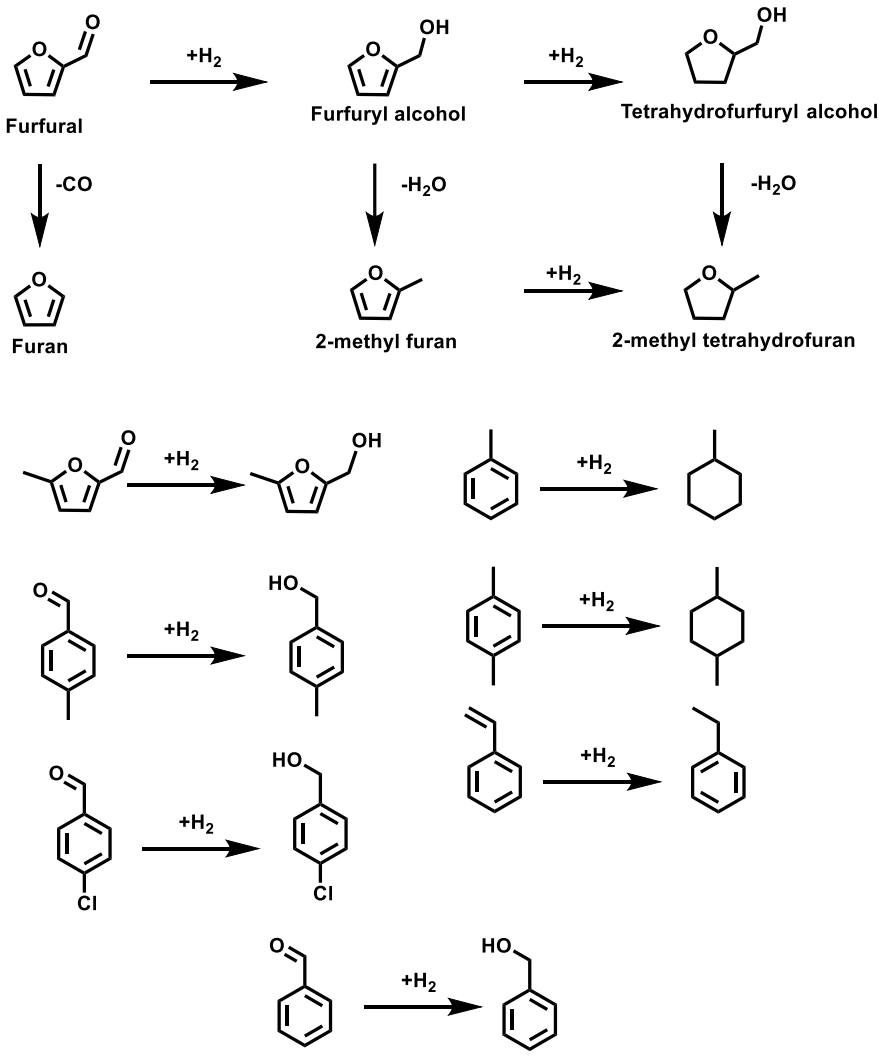

Figure S29. Reaction networks for the reactions depicted in figures 2a, 2c, and 2d.

Table S1. Textural properties of HCP, Ir-HCP, Si-Beta, and ZSM-5.

Sample	S_{BET} (m^2g^{-1}) [a]	D_{pore} (nm) [b]	V_{pore} (cm^3g^{-1})[c]	N (wt%)[d]	C (wt%)[d]	H(wt%)[d]
HCP-CH_3	**720**	**2.8**	**0.49**	**0.71**	**76.33**	**6.76**
HCP-OH	**324**	**3.5**	**0.29**	**0.70**	**84.54**	**8.64**
Ir-HCP-CH_3	**701**	**2.7**	**0.47**	**0.72**	**80.51**	**6.41**
Ir-HCP-OH	**253**	**3.8**	**0.24**	**0.77**	**78.90**	**6.78**
Si-BETA	**511**	**0.84**	**0.24**	**-**	**-**	**-**
Si-ZSM-5	**334**	**0.80**	**0.15**	**-**	**-**	**-**

[a] Calculated with the multipoint BET equation. [b] Pore width calculated with the NLDFT model. [c] Total pore volume calculated at P/P_0 = 0.99. [d] Determined by elemental analysis.

Table S2. Adsorption area of cyclopentanone, cyclohexanone, and cycloheptanone on Si-Beta and Si-ZSM-5.

	Area (cm^{-1})			Comparable Area[a]		
	Cyclo-pentanone	Cyclo-hexanone	Cyclo-heptanone	Cyclo-pentanone	Cyclo-hexanone	Cyclo-heptanone
Si-Beta	**74.84**	**84.4**	**89.6**	**92.8**	**84.4**	**166.7**
Si-ZSM-5	**9.46**	**7.55**	**2.15**	**11.73**	**7.55**	**3.99**

a, comparable area calculate

cyclopentanone:cyclohexanone:cycloheptanone = 1.23： 1:1.86

Table S3. Adsorption energies (E_{ads}) of furfural over OH group and CH_3 group on the zigzag model and armchair model.

E_{ads} of furfural	**Zigzag model**	**Armchair model**
OH group	**-0.40 eV**	**-0.47 eV**
CH_3 group	**-0.33 eV**	**-0.31 eV**

Table S4. Comparation of recent works on furfural hydrogenation modulation.

Entry	Catalyst	Active site	Main products	Method to modulate catalytic performance	Method	Ref.
1	OH functional HCPs supported Ir	Ir	Furfural alcohol	Hydrogen bond interaction	Experiment + DFT	This work
2	Organic modified Pd/TiO_2	Pd	Furfural alcohol	Surface active site modulation	Experiment	[1]
3	Co-impregnation of Pd and Ir on SiO_2	Ir,Pd	Furfural alcohol and tetrahydrofurfuryl alcohol	Metal alloy method	Experiment	[2]
4	Pt(111), stepped Pt(211), and Pt55 cluster	Pt	Furfural alcohol and furan	Particle size	DFT	[3]
5	sol-immobilization Pd/TiO_2	Pd	Furfural alcohol and tetrahydrofurfuryl alcohol	Particle size and active site	Experiment + DFT	[4]
6	α-MoC	α-MoC	Methyl furan	Solvent	Experiment + DFT	[5]
7	Phosphoric acid modified Pt/Al2O3	Pt	Methyl furan	Interfacial Metal-acid site	Experiment	[6]
8	Pd(111)	Pd	Furfuryl alcohol or furan	Hydrogen-coverage	DFT	[7]

Supplementary Note 1

In order to test the universality of the H bond in other materials except the special designed POPs, we tested the adsorption of ketones on Si- Beta and Si-ZSM-5 using *in-situ* FT-IR (Figure S27). Three different ketones with different molecule size including cyclopentanone, cyclohexanone, and cycloheptanone were tested. Irrespective of the substrate, Si-Beta adsorbs almost 10× than Si-ZSM-5 (Table S2). Although the two zeolites differ in BET surface area, pore volume, and pore size (Table S1), these little differences cannot explain such a huge adsorption difference. DRIFTS-IR reveals a huge difference in the area around 3500 cm^{-1} (Figure S28), ascribed to Si-OH groups, implying many more OH groups in Si-Beta than Si-ZSM-5 that can hydrogen bond with the carbonyl groups. which can form the hydrogen bond between the carbonyl groups and the Si-OH. It is highly believed that this is the main reason for the huge adsorption difference. This experiment demonstrated weak interaction like H bond might widely existed in during the

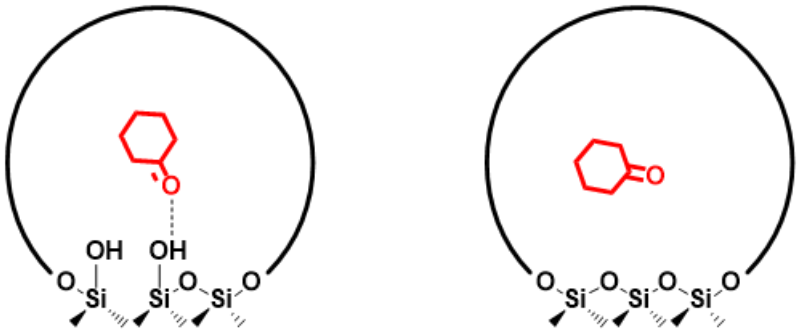

Illustration of hydrogen bond formed between ketone and Si-OH in zeolite pores.

Supplementary References

1. Pang SH, Schoenbaum CA, Schwartz DK, Medlin JW. Effects of Thiol Modifiers on the Kinetics of Furfural Hydrogenation over Pd Catalysts. ACS Catalysis 4, 3123-3131 (2014).

2. Nakagawa Y, Takada K, Tamura M, Tomishige K. Total Hydrogenation of Furfural and 5-Hydroxymethylfurfural over Supported Pd–Ir Alloy Catalyst. ACS Catalysis 4, 2718-2726 (2014).

3. Cai Q-X, Wang J-G, Wang Y-G, Mei D. Mechanistic insights into the structure-dependent selectivity of catalytic furfural conversion on platinum catalysts. AIChE Journal 61, 3812-3824 (2015).

4. Rogers SM, et al. Tandem Site- and Size-Controlled Pd Nanoparticles for the Directed Hydrogenation of Furfural. ACS Catalysis 7, 2266-2274 (2017).

5. Deng Y, et al. Solvent Tunes the Selectivity of Hydrogenation Reaction over α-MoC Catalyst. Journal of the American Chemical Society 140, 14481-14489 (2018).

6. Zhang J, et al. Control of interfacial acid–metal catalysis with organic monolayers. Nature Catalysis 1, 148-155 (2018).

7. Wang S, Vorotnikov V, Vlachos DG. Coverage-Induced Conformational Effects on Activity and Selectivity: Hydrogenation and Decarbonylation of Furfural on Pd(111). ACS Catalysis 5, 104-112 (2015).